THE JOURNAL OF PHYSICAL CHEMISTRY LETTERS
A JOURNAL OF THE AMERICAN CHEMICAL SOCIETY

pubs.acs.org/JPCL Letter

Greatly Enhanced Raman Scattering of Graphene on Metals by a Boron Nitride Film Covering

Chang Liu,[○] Chaojie Ma,[○] Dewei Gong,[○] Chenjun Ma, Dongxue Chen, Chunchun Wu, Mengze Zhao, Zhibin Zhang, Jinming Yun, Fajun Xiao, EnGe Wang, Kaihui Liu,* and Hao Hong*

Cite This: *J. Phys. Chem. Lett.* 2023, 14, 5573−5579 Read Online

ACCESS | Metrics & More | Article Recommendations | Supporting Information

ABSTRACT: Raman spectroscopy, a nondestructive fingerprinting technique, is mainly utilized to identify molecular species and phonon modes of materials. However, direct Raman characterization of two-dimensional materials typically synthesized on catalytic metal substrates is extremely challenging because of the significant electric screening and interfacial electronic couplings. Here, we demonstrate that by covering as-grown graphene with boron nitride (BN) films, the Raman intensity of graphene can be enhanced by two orders of magnitude and is also several times stronger than that of suspended graphene. This great Raman enhancement originates from the optical field amplification by Fabry−Pérot cavity in BN films and the local field plasmon near copper steps. We further demonstrate the direct characterization of the local strain and doping level of as-grown graphene and *in situ* monitoring of the molecule reaction process by enhanced Raman spectroscopy. Our results will broaden the optical investigations of interfacial sciences on metals, including photoinduced charge transfer dynamics and photocatalysis at metal surfaces.

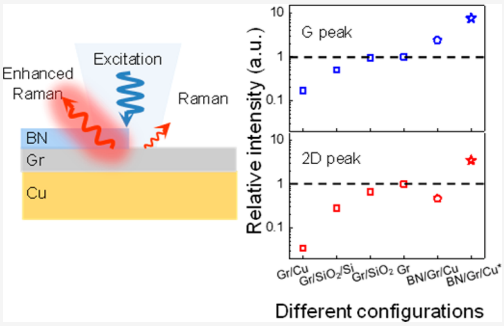

Graphene has attracted intensive research interest and exhibited great potential in electronic, optoelectronic, and nanomechanical applications due to its exceptional properties, including its intriguing Dirac band structure,[1−4] unique hot carrier dynamic processes,[5−8] superior mechanical strength,[9−11] etc. For practical applications, high-quality graphene with a large area is a prerequisite and relies on the accompanying high-throughput synthesis and quality inspection. Generally, the synthesis of monolayer graphene on a catalytic metal substrate (such as copper foil) by the chemical vapor deposition (CVD) method has been well developed,[12−16] yet a reliable *in situ* characterization method still remains immature. Among the abundant characterization technologies, including X-ray diffraction, low-energy electron diffraction, and scanning transmission electron microscopy, Raman spectroscopy is highly promising with the merits of nondestructive characterization and high efficiency.[17−25] However, Raman signals from graphene are typically very weak due to the nature of the inelastic scattering process, as well as the atomic-thick light−matter interaction length. Especially for as-grown graphene on metal substrates, the optical signals including Raman signals will be further reduced by the significant electric screening effect from the metal beneath. The strong interfacial coupling would also worsen the situation by hybridizing the electronic states of materials with d-orbital electrons from metals and strongly modify the Raman signal.[26−28]

Previously, lots of routes have been developed to boost the Raman signals by physical and chemical enhancement, such as surface-enhanced Raman spectroscopy[29−32] and tip-enhanced Raman spectroscopy,[33−35] etc. However, those methods are in need of designed substrates or metal tips producing a local electromagnetic field hot spot, which are not suitable to realize *in situ* Raman characterization of as-grown graphene on various metal substrates under different circumstances. Chemical enhancement holds the merit of the independence of the electromagnetic environment, while the elusive mechanism of the complex charge transfer process hinders its practical design and application.[36−39] Other methods such as conducting Raman spectroscopy by tuning the excitation laser energy[40−42] or spontaneous oxidation of the underlying copper substrate[43] only exhibit Raman enhancement of several times. The oxidation process is also not applicable for noble metals such as gold and platinum. As for conducting a transfer process to remove the metal substrates, the samples could be transferred onto substrates such as silicon dioxides/silicon (SiO_2/Si) with a certain oxidation layer thickness.[44] However, such a transfer process is complex and would inevitably introduce defects, wrinkles, or contaminants to the samples. A facile but efficient enhancement method is still needed to directly conduct *in situ*

Received: April 20, 2023
Accepted: June 6, 2023
Published: June 12, 2023

Downloaded via PEKING UNIV on July 3, 2023 at 12:56:03 (UTC).
See https://pubs.acs.org/sharingguidelines for options on how to legitimately share published articles.

ACS Publications © 2023 American Chemical Society

https://doi.org/10.1021/acs.jpclett.3c01074
J. Phys. Chem. Lett. 2023, 14, 5573−5579

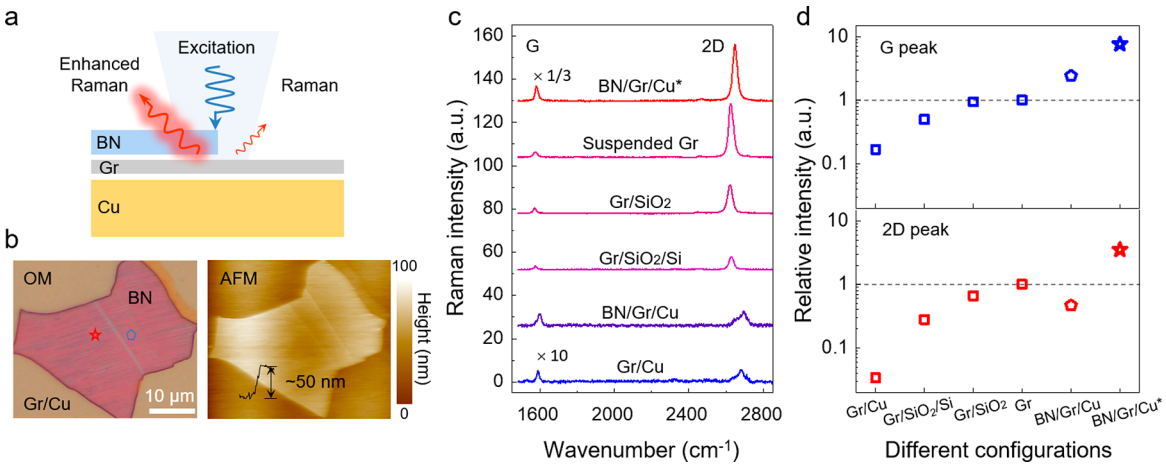

Figure 1. Raman enhancement by BN film covering. (a) Schematic representation of optical field amplification by a BN film covering on as-grown graphene on a copper substrate. (b) Optical microscope (OM) and atomic force microscope (AFM) images of the representative BN/Gr/Cu sample characterized in our experiment. The thickness of the BN film is about 50 nm. The red and blue marks on the OM image represent the two different sample configurations near and away from the copper step, respectively. (c) Raman intensity of graphene in various configurations, including Gr/Cu, Gr/SiO_2/Si, Gr/SiO_2, Gr (suspended), BN/Gr/Cu (terrace), and BN/Gr/Cu* (copper step). By covering Gr/Cu with BN (thickness ∼50 nm), the Raman intensity of graphene, including both G and 2D peaks, is greatly enhanced. (d) Relative Raman intensity of graphene (both G and 2D peaks) normalized with respect to that of suspended graphene extracted from (c), showing great Raman enhancement in the BN/Gr/Cu and BN/Gr/Cu* configurations.

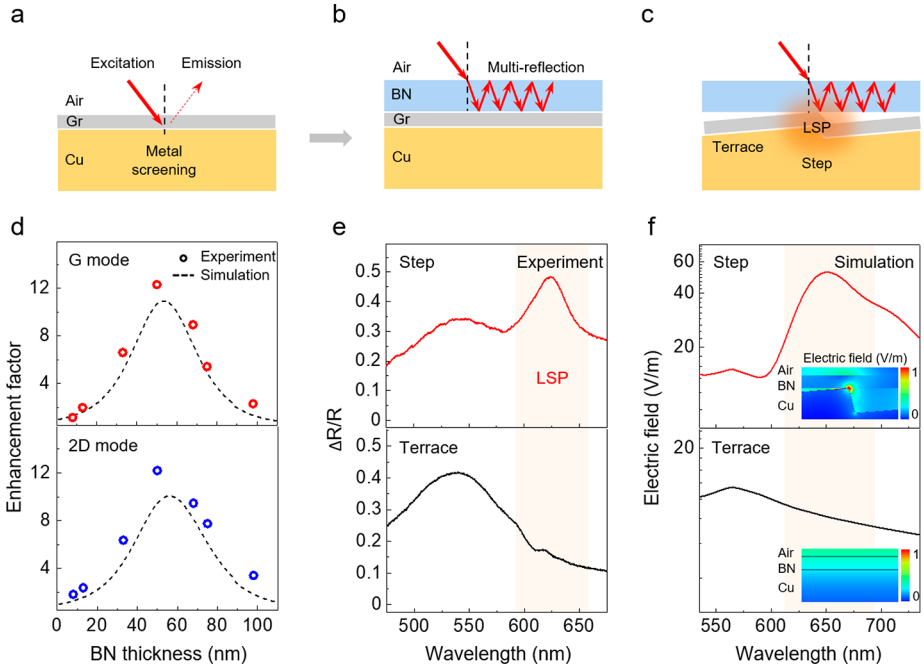

Figure 2. Mechanism of Raman enhancement by a BN film covering. (a−c) Schematic diagrams showing (a) the metal screening effect from copper, (b) the optical field amplification resulting from multireflection, and (c) LSP enhancement under laser excitation. With the BN film covering, the interferential F−P cavity formed between the air/BN and BN/Cu interface greatly enhanced the optical field near graphene, thus resulting in the Raman emission enhancement. Besides, the optical field will be further amplified near the copper step due to the LSP effect. (d) Experimental (circle) and simulated (dashed lines) Raman enhancement factors by the BN film covering as a function of the BN thickness. Both the G and 2D modes show the largest enhancement factor with a BN thickness of ∼55 nm. (e) Experimental and (f) simulated results to clarify the LSP effect near the copper step. It is evident that the copper step structure brings about more resonance peaks than the terrace structure, which leads to the further enhanced Raman intensity.

Raman characterization of as-grown graphene on metal substrates.

Here we demonstrate that great and uniform Raman enhancement can be achieved on metal substrates by covering as-grown graphene on copper with boron nitride (BN) films. The interface between air/BN and BN/metal surface forms an interferential Fabry−Pérot (F−P) cavity to realize optical field enhancement. Together with plasmonic local field enhancement near the copper step, the Raman intensity of graphene can be enhanced by about two orders of magnitude compared to that of bare graphene on copper. The local strain distribution and doping level of graphene grown on copper

https://doi.org/10.1021/acs.jpclett.3c01074
J. Phys. Chem. Lett. 2023, 14, 5573−5579

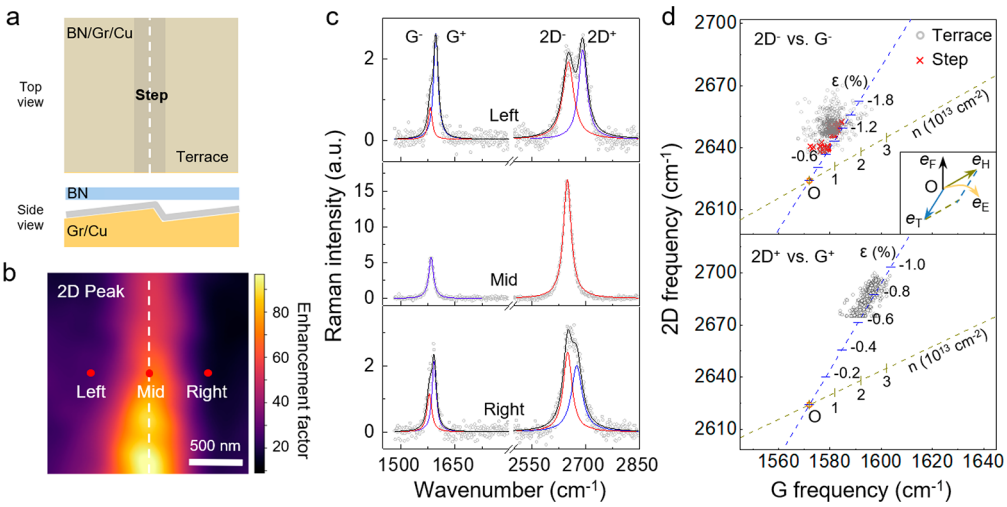

Figure 3. Local strain and doping characterization of graphene by enhanced Raman near the copper step. (a) Schematic diagram showing the top view and cross section of BN/Gr/Cu near the copper step (white dashed line). (b) Enhancement factor mapping of the graphene 2D Raman mode in BN/Gr/Cu near the copper step. The Raman intensity on the copper step can be enhanced by about two orders of magnitude compared to bare Gr/Cu after BN covering. The three red marks correspond to the left, middle, and right Raman spectra in (c), respectively. (c) Enhanced Raman spectra of graphene on the copper terrace (left and right, with a configuration of BN/Gr/Cu) and step (middle, with a configuration of BN/Gr/Cu*). It is clear that the graphene Raman spectrum on the step has a good single peak fitting feature, accompanied by stronger emission intensity. (d) Correlation between the frequencies of G and 2D Raman modes of graphene on the copper terrace (gray circle) and the copper step (red cross). G^- (G^+) and $2D^-$ ($2D^+$) modes correspond to the lower (higher) frequency mode of the G and the 2D mode, respectively. The orange circle represents the graphene Raman frequency from the suspended graphene that is not affected by strain and doping. The blue dashed line is the prediction of G and 2D frequency for charge-neutral graphene under randomly oriented uniaxial strain, and the blue bar on it designates strain ranging from 0% to −1.8%. The olive dashed line is the hole-doping-induced Raman frequency change without strain, and the bar on it marks the hole doping level. Inset: decomposition of all the effects using a vector model, including hole-doping vector $\boldsymbol{e}_H$, electron doping vector $\boldsymbol{e}_E$, tensile strain vector $\boldsymbol{e}_T$, and Fermi velocity reduction vector $\boldsymbol{e}_F$.

can be clearly resolved *in situ* with the enhanced Raman signals. This facile method can serve as a robust Raman enhancement tool for other low-dimensional materials and chemical molecules, including MoS_2 on gold, R6G molecules, and even a molecular reaction on copper.

In our experiment, graphene was synthesized using CVD on Cu(111) substrates. Then, BN films with a uniform thickness were transferred onto as-grown graphene by dry transfer methods (Figure 1a, see Methods for details). The typical thickness of the covered BN film is about 50 nm, as characterized by atomic force microscope (AFM) mapping (Figure 1b). Raman spectra of graphene on copper (Gr/Cu), BN−covered graphene on copper (BN/Gr/Cu), and other configurations, including graphene on SiO_2 (300 nm)/Si (Gr/SiO_2/Si), graphene on fused silica (Gr/SiO_2), and suspended graphene (suspended Gr, Figure S1), upon laser excitation of 633 nm are shown in Figure 1c for comparison. In contrast to the spectrum of suspended graphene, both the Raman G mode and 2D mode of Gr/Cu split into two peaks and exhibit a dramatic decrease in intensity, while the Raman spectrum of BN/Gr/Cu* with the BN film covering near the copper step (the copper step is known as the corrugated morphology of copper surface formed during the graphene growth by step bunching process, which is inevitable and widespread on metal surfaces) exhibits a pretty good line shape and strong intensity (Figure 1c). To directly compare the Raman intensity, we calculated the Raman enhancement factor in Figure 1d. In the BN/Gr/Cu configuration, the Raman intensities of graphene have been enhanced by a factor of ∼13 for both modes compared to those in bare Gr/Cu. Strikingly, in BN/Gr/Cu*, the Raman enhancement increases to ∼50−100, with intensity also stronger than that of suspended graphene (Figure 1d).

The position-dependent enhanced Raman signals inspire us to analyze the enhancement effects by studying configurations of BN/Gr/Cu and BN/Gr/Cu* separately. As for the BN/Gr/Cu configuration, the air/BN and BN/Cu interfaces form an interferential F−P cavity, resulting in the optical field enhancement near the graphene layer (Figure 2b). As the interference condition of a F−P cavity is a function of the laser wavelength and the cavity length, the enhancement factor varies correspondingly with the BN thickness and excitation wavelength (Figure S2). Both G and 2D peaks show the largest enhancement factor with a BN thickness of ∼55 nm from experimental and simulation results (Figure 2d). Similar Raman enhancements were also observed in the configurations of TiO_2/Gr/Cu and $MoSe_2$/Gr/Cu (Figure S3).

As for the BN/Gr/Cu* configuration near the copper step, besides F−P cavity amplification, the nanosized step edge produces an additional optical field enhancement from the local surface plasmon (LSP) effect (Figure 2c). Using reflection contrast spectra, we experimentally find a resonance peak in a typical BN/Gr/Cu* sample (Figure 2e). This LSP resonant peak is closely related to the structure of the copper step, as characterized from our more than 20 samples. Our excitation wavelength (633 nm) correctly locates in the LSP resonance peak range of 600−650 nm and thus the Raman is further enhanced by nearly two orders of magnitude. Moreover, the Raman intensity of BN/Gr/Cu* exhibits a polarization-dependent behavior closely related to the orientation of copper step, which is a standard feature of the LSP effect[45,46] (Figure S4). As the Raman intensities from bare Gr/Cu and Gr/Cu* are almost the same, the greatly enhanced Raman intensity from BN/Gr/Cu* corresponds to the formation of LSP by the coverage of BN film (Figure S5).

https://doi.org/10.1021/acs.jpclett.3c01074
J. Phys. Chem. Lett. 2023, 14, 5573−5579

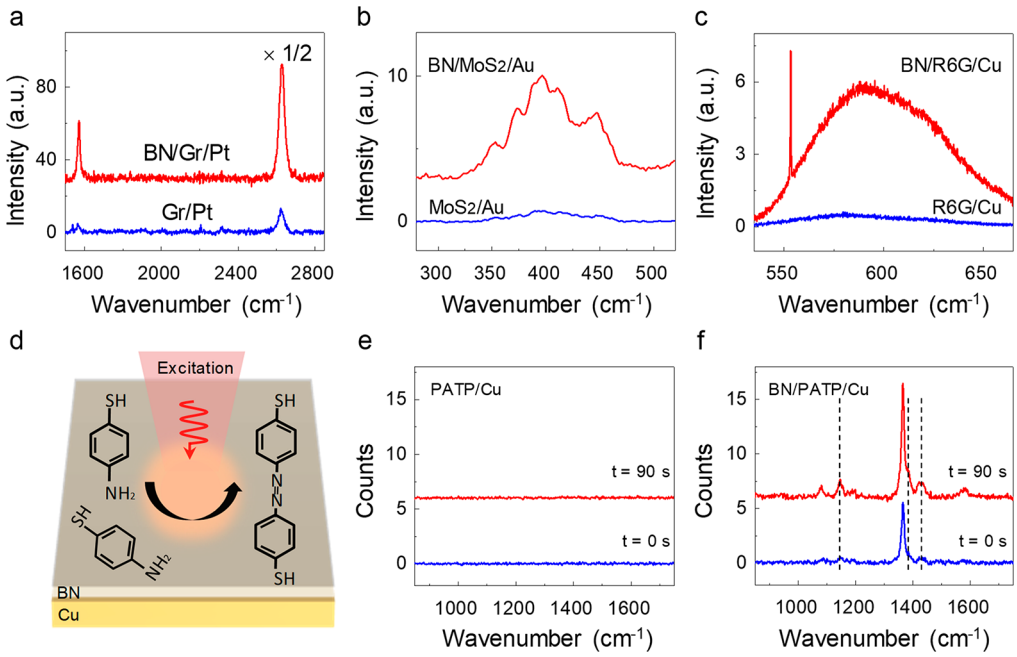

Figure 4. Universal Raman enhancement of low-dimensional materials on various metal substrates. (a and b) Raman intensity enhancement of (a) Gr/Pt and (b) MoS_2/Au by the BN film covering. (c) PL intensity enhancement of R6G molecules on the copper substrate by the BN film covering. (d−f) *In situ* monitoring reaction process of PATP molecules by Raman under laser excitation on the copper substrate (d). On bare PATP/Cu, the Raman signals of molecules can hardly be observed (e). While with BN film covering, the PATP molecule reaction process can be clearly monitored by the Raman intensity (f).

This highly agrees with our simulation results, where the copper step structure in the BN/Gr/Cu* configuration brings about a local optical field hot spot near the step edge (Figure 2f).

During the graphene synthesis process on metal surface, substrate-induced strain is ubiquitous because of the discrepancy in the thermal expansion coefficient between graphene and metal[47−50] (*e.g.*, copper has a thermal expansion coefficient of ∼2 × 10^{-5} K^{-1}, while graphene has a negative and almost negligible coefficient). The enhanced Raman signal of the BN/Gr/Cu configuration directly provides us the opportunity to characterize the local strain together with doping information on as-grown graphene on a copper substrate.[18−23] By conducting Raman mapping (Figure 3a and b), the clearly resolved Raman peak splitting and shifting will illustrate the detailed strain and doping level. Three Raman spectra (marked by red dots in Figure 3b) around BN/Gr/Cu* are shown in Figure 3c. In the positions away from the step (the left and right points in Figure 3b with the configuration of BN/Gr/Cu), both G and 2D peaks split into two components with lower/higher frequency, denoted by G^-/G^+ and $2D^-/2D^+$, respectively. The Raman peak splitting of the G and 2D modes indicates the uniaxial strain in the graphene lattice. In the position of the step (the middle points in Figure 3b with a configuration of BN/Gr/Cu*), both G and 2D peaks of graphene exhibit pretty good single peak features with lower frequencies (Figure 3c).

The strain (ε) and doping of as-grown graphene on a copper substrate can be analyzed by the correlation between frequencies of the G and 2D modes using vector analysis (*i.e.*, "strain-free" vector $\boldsymbol{e}_H$ for hole doping and "charge-neutral" vector $\boldsymbol{e}_T$ for tensile strain, as shown in the inset of Figure 3d). The suspended monolayer graphene sample without the influence of strain and the doping effect was investigated for comparison (Figure S1), with the G mode at 1572 cm^{-1} and the 2D mode at 2624 cm^{-1} (orange circle (O) in Figure 3d). The blue-shifted Raman peaks of graphene in BN/Gr/Cu indicate the strain is compressive. By conducting correlated analysis of the $G^-(G^+)$ and $2D^-(2D^+)$ peaks, the strain and doping level of graphene can be investigated separately. The blue dashed lines in Figure 3d indicate the randomly oriented uniaxial strain effect without charge doping (with slopes $\Delta\omega_{2D}/\Delta\omega_G$ = 1.97 and 2.5 for $2D^-/G^-$ and for $2D^+/G^+$, respectively), while the olive dashed lines indicate the hole doping effect without strain (with a slope $\Delta\omega_{2D}/\Delta\omega_G$ = 0.7).[23] Notably, the Raman data dots from the mapping area of a typical BN/Gr/Cu* sample (Figure S2) distribute well along blue dashed lines. After statistical analysis (Figures 3d and S6), we can obtain the compressive strain to be about −0.77% (−0.76%) with a standard deviation of 0.26% (0.085%) for the G^- (G^+) mode. Remarkably, the Raman data sets of two different steps (red cross in Figure 3d) tend to concentrate into two groups (centered at around −0.65% and −0.95%, respectively, Figure S6c), indicating the distinct build-up strain and strain relaxation results for different copper steps. Unlike the strain relaxation results in graphene wrinkles where the strain is believed to be released,[49] it is the release of local bending energy of graphene (not the compressive strain) that drives the step-bunching process in the vicinity of surface steps on the copper.[50]

As for the doping effect, the change of ($\Delta\omega_{2D}/\Delta\omega_G$) is determined by the sign of the charges. However, either hole (vector $\boldsymbol{e}_H$) or electron (vector $\boldsymbol{e}_E$) doping would lead to smaller slopes of ($\Delta\omega_{2D}/\Delta\omega_G$), which is not sufficient in our experiments ($n < 1 \times 10^{13}$ cm^{-2}). The slight upshift of the data set distribution compared with the dashed line can be attributed to the existence of an interlayer van der Waals interaction between graphene and BN, which modifies the

https://doi.org/10.1021/acs.jpclett.3c01074
J. Phys. Chem. Lett. 2023, 14, 5573−5579

Fermi velocity of graphene and results in an increase in ω_{2D} (corresponding to the vector of e_F).[25]

Due to the effective Raman enhancement mechanism of cavity amplification and LSP effects, the coverage of the BN film could serve as a universal enhancement tool on the metal surfaces. For example, it is pretty convenient to obtain an enhanced Raman spectrum of graphene on platinum substrate (Gr/Pt), as well as MoS_2 on a gold substrate (MoS_2/Au), by covering the sample with BN films (Figure 4a and b). What's more, the amplified optical field intensity could lead to the enhancement of other optical responses, such as photoluminescence (PL) of R6G molecules (Figure 4c).

Enhanced optical signals for molecules enable us to monitor the molecule reaction process *in situ*. We choose *p*-aminothiophenol (PATP) molecules as the reactants and monitored the laser-induced chemical transformation to *p*,*p*′-dimercaptoazobenzene (DMAB) molecules[51,52] (Figure 4d). In our experiment, the copper substrate was first soaked in the ethanol solution of PATP at a low concentration (10^{-3} mol/L) and then covered with the BN film. As for bare PATP/Cu, the Raman signals of the PATP and DMAB molecules can hardly be detected under laser illumination (Figure 4e), while with BN film coverage the laser-induced PATP to DMAB reaction process can be clearly characterized by the emergence of product Raman signals (such as those at 1146, 1377, and 1425 cm^{-1}) (Figure 4f). In this design, the BN/PATP/Cu configuration plays the role of facilitating the chemical reaction process as well as enhancing the Raman signals of molecules, as the excitation optical field has been enhanced.

In conclusion, we have developed an effective and robust method of BN film covering to achieve Raman enhancement for low-dimensional materials on various metal substrates, including Gr/Cu, Gr/Pt, MoS_2/Au, and molecules on a metal surface. The Raman emission of graphene can be enhanced by about two orders of magnitude *in situ* on a copper substrate. Given the universality of our approach, the enhanced optical field from the BN film covering can be widely utilized for optical investigations of interfacial sciences on metals in combination with time-resolved spectroscopy, such as photo-induced charge carrier dynamics at metal surfaces, and electron dynamics in metal nanostructures.

■ METHODS

Sample Preparation. The graphene was synthesized by CVD. A cooper foil was first placed on a quartz substrate and loaded into the CVD furnace. Then the system was heated to 1040 °C under a reducing atmosphere of 500 standard cubic centimeters per minute (sccm) Ar and 30 sccm H_2. After the sample was held at 1040 °C for 1 h to obtain single crystal copper foil, 0.01 sccm/10 sccm of CH_4/H_2 was introduced into the system for 10−30 min to obtain graphene on copper (Gr/Cu). The BN films deposited on Gr/Cu were mechanically exfoliated from the bulk and then underwent with transfer process (Figure S7).

Raman Characterization. Raman spectra and mappings were collected by a Horiba system (iHR-550) with excitation wavelengths of 633 and 532 nm. As for the polarization dependence measurement, the Raman spectra were collected by a Witec system (Alpha-700R) with an excitation wavelength of 514 nm by rotating the incident polarization. All the Raman spectra analyzed in the main text are under the excitation of 633 nm unless otherwise stated.

Simulation. Numerical simulations were processed using the Wave Optics Module of COMSOL Multiphysics software. The intensity of the electric field was calculated using the finite element method in COMSOL.

■ ASSOCIATED CONTENT

Supporting Information

The Supporting Information is available free of charge at https://pubs.acs.org/doi/10.1021/acs.jpclett.3c01074.

Additional experimental results (PDF)

■ AUTHOR INFORMATION

Corresponding Authors

Kaihui Liu − *International Centre for Quantum Materials, Collaborative Innovation Centre of Quantum Matter, Peking University, Beijing 100871, China; State Key Laboratory for Mesoscopic Physics, Frontiers Science Centre for Nano-Optoelectronics, School of Physics, Peking University, Beijing 100871, China; Peking University Yangtze Delta Institute of Optoelectronics, Nantong, Jiangsu 226000, China;* orcid.org/0000-0002-8781-2495; Email: khliu@pku.edu.cn

Hao Hong − *State Key Laboratory for Mesoscopic Physics, Frontiers Science Centre for Nano-Optoelectronics, School of Physics and Interdisciplinary Institute of Light-Element Quantum Materials and Research Centre for Light-Element Advanced Materials, Peking University, Beijing 100871, China*; Email: haohong@pku.edu.cn

Authors

Chang Liu − *International Centre for Quantum Materials, Collaborative Innovation Centre of Quantum Matter, Peking University, Beijing 100871, China;* orcid.org/0000-0002-6273-6465

Chaojie Ma − *State Key Laboratory for Mesoscopic Physics, Frontiers Science Centre for Nano-Optoelectronics, School of Physics, Peking University, Beijing 100871, China;* orcid.org/0000-0003-3649-5220

Dewei Gong − *State Key Laboratory for Mesoscopic Physics, Frontiers Science Centre for Nano-Optoelectronics, School of Physics, Peking University, Beijing 100871, China*

Chenjun Ma − *State Key Laboratory for Mesoscopic Physics, Frontiers Science Centre for Nano-Optoelectronics, School of Physics, Peking University, Beijing 100871, China*

Dongxue Chen − *State Key Laboratory for Mesoscopic Physics, Frontiers Science Centre for Nano-Optoelectronics, School of Physics, Peking University, Beijing 100871, China*

Chunchun Wu − *State Key Laboratory for Mesoscopic Physics, Frontiers Science Centre for Nano-Optoelectronics, School of Physics, Peking University, Beijing 100871, China;* orcid.org/0000-0002-4334-6744

Mengze Zhao − *State Key Laboratory for Mesoscopic Physics, Frontiers Science Centre for Nano-Optoelectronics, School of Physics, Peking University, Beijing 100871, China*

Zhibin Zhang − *State Key Laboratory for Mesoscopic Physics, Frontiers Science Centre for Nano-Optoelectronics, School of Physics, Peking University, Beijing 100871, China*

Jinming Yun − *Shaanxi Key Laboratory of Optical Information Technology, School of Physical Science and Technology, Northwestern Polytechnical University, Xi'an, Shaanxi 710072, China*

https://doi.org/10.1021/acs.jpclett.3c01074
J. Phys. Chem. Lett. 2023, 14, 5573−5579

Fajun Xiao − *Shaanxi Key Laboratory of Optical Information Technology, School of Physical Science and Technology, Northwestern Polytechnical University, Xi'an, Shaanxi 710072, China;* orcid.org/0000-0002-7656-7869

EnGe Wang − *International Centre for Quantum Materials, Collaborative Innovation Centre of Quantum Matter, Peking University, Beijing 100871, China; Songshan Lake Materials Laboratory, Dongguan, Guangdong 523808, China; Department of Physics, Shanghai University, Shanghai 200444, China*

Complete contact information is available at: https://pubs.acs.org/10.1021/acs.jpclett.3c01074

Author Contributions

○These authors contributed equally to this work.

Notes

The authors declare no competing financial interest.

■ ACKNOWLEDGMENTS

This work was supported by the Guangdong Major Project of Basic and Applied Basic Research (2021B0301030002), the National Natural Science Foundation of China (12104018, 52025023, 51991342, 52021006, 92163206, 11888101, and T2188101), the National Key R&D Program of China (2022YFA1403504, 2021YFA1400201, and 2021YFA1400502), and the China Postdoctoral Science Foundation (2022M710232, 2020M680177, 2021T140022).

■ REFERENCES

(1) Novoselov, K. S.; Geim, A. K.; Morozov, S. V.; Jiang, D.; Katsnelson, M. I.; Grigorieva, I. V.; Dubonos, S. V.; Firsov, A. A. Two-Dimensional Gas of Massless Dirac Fermions in Graphene. *Nature* **2005**, *438*, 197−200.

(2) Zhang, Y. B.; Tan, Y. W.; Stormer, H. L.; Kim, P. Experimental Observation of the Quantum Hall Effect and Berry's Phase in Graphene. *Nature* **2005**, *438*, 201−204.

(3) Castro Neto, A. H.; Guinea, F.; Peres, N. M. R.; Novoselov, K. S.; Geim, A. K. The Electronic Properties of Graphene. *Rev. Mod. Phys.* **2009**, *81*, 109−162.

(4) Xu, X. Z.; Liu, C.; Sun, Z. H.; Cao, T.; Zhang, Z. H.; Wang, E. G.; Liu, Z. F.; Liu, K. H. Interfacial Engineering in Graphene Bandgap. *Chem. Soc. Rev.* **2018**, *47*, 3059−3099.

(5) Xia, F. N.; Mueller, T.; Lin, Y. M.; Valdes-Garcia, A.; Avouris, P. Ultrafast Graphene Photodetector. *Nat. Nanotechnol* **2009**, *4*, 839−843.

(6) Bonaccorso, F.; Sun, Z.; Hasan, T.; Ferrari, A. C. Graphene Photonics and Optoelectronics. *Nat. Photonics* **2010**, *4*, 611−622.

(7) Johannsen, J. C.; Ulstrup, S.; Cilento, F.; Crepaldi, A.; Zacchigna, M.; Cacho, C.; Turcu, I. C. E.; Springate, E.; Fromm, F.; Raidel, C.; et al. Direct View of Hot Carrier Dynamics in Graphene. *Phys. Rev. Lett.* **2013**, *111*, 027403.

(8) Koppens, F. H. L.; Mueller, T.; Avouris, P.; Ferrari, A. C.; Vitiello, M. S.; Polini, M. Photodetectors Based on Graphene, Other Two-Dimensional Materials and Hybrid Systems. *Nat. Nanotechnol* **2014**, *9*, 780−793.

(9) Lee, C.; Wei, X. D.; Kysar, J. W.; Hone, J. Measurement of the Elastic Properties and Intrinsic Strength of Monolayer Graphene. *Science* **2008**, *321*, 385−388.

(10) Geim, A. K. Graphene: Status and Prospects. *Science* **2009**, *324*, 1530−1534.

(11) Kim, K. S.; Zhao, Y.; Jang, H.; Lee, S. Y.; Kim, J. M.; Kim, K. S.; Ahn, J. H.; Kim, P.; Choi, J. Y.; Hong, B. H. Large-Scale Pattern Growth of Graphene Films for Stretchable Transparent Electrodes. *Nature* **2009**, *457*, 706−710.

(12) Wang, H.; Wang, G. Z.; Bao, P. F.; Yang, S. L.; Zhu, W.; Xie, X.; Zhang, W. J. Controllable Synthesis of Submillimeter Single-Crystal Monolayer Graphene Domains on Copper Foils by Suppressing Nucleation. *J. Am. Chem. Soc.* **2012**, *134*, 18476−18476.

(13) Yan, Z.; Lin, J.; Peng, Z. W.; Sun, Z. Z.; Zhu, Y.; Li, L.; Xiang, C. S.; Samuel, E. L.; Kittrell, C.; Tour, J. M. Toward the Synthesis of Wafer-Scale Single-Crystal Graphene on Copper Foils. *ACS Nano* **2012**, *6*, 9110−9117.

(14) Hao, Y. F.; Bharathi, M. S.; Wang, L.; Liu, Y. Y.; Chen, H.; Nie, S.; Wang, X. H.; Chou, H.; Tan, C.; Fallahazad, B.; et al. The Role of Surface Oxygen in the Growth of Large Single-Crystal Graphene on Copper. *Science* **2013**, *342*, 720−723.

(15) Xu, X. Z.; Zhang, Z. H.; Qiu, L.; Zhuang, J. N.; Zhang, L.; Wang, H.; Liao, C. N.; Song, H. D.; Qiao, R. X.; Gao, P.; et al. Ultrafast Growth of Single-Crystal Graphene Assisted by a Continuous Oxygen Supply. *Nat. Nanotechnol* **2016**, *11*, 930−935.

(16) Xu, X. Z.; Zhang, Z. H.; Dong, J. C.; Yi, D.; Niu, J. J.; Wu, M. H.; Lin, L.; Yin, R. K.; Li, M. Q.; Zhou, J. Y.; et al. Ultrafast Epitaxial Growth of Metre-Sized Single-Crystal Graphene on Industrial Cu Foil. *Sci. Bull.* **2017**, *62*, 1074−1080.

(17) Malard, L. M.; Pimenta, M. A.; Dresselhaus, G.; Dresselhaus, M. S. Raman Spectroscopy in Graphene. *Phys. Rep.* **2009**, *473*, 51−87.

(18) Das, A.; Pisana, S.; Chakraborty, B.; Piscanec, S.; Saha, S. K.; Waghmare, U. V.; Novoselov, K. S.; Krishnamurthy, H. R.; Geim, A. K.; Ferrari, A. C.; et al. Monitoring Dopants by Raman Scattering in an Electrochemically Top-Gated Graphene Transistor. *Nat. Nanotechnol* **2008**, *3*, 210−215.

(19) Mohiuddin, T. M. G.; Lombardo, A.; Nair, R. R.; Bonetti, A.; Savini, G.; Jalil, R.; Bonini, N.; Basko, D. M.; Galiotis, C.; Marzari, N.; et al. Uniaxial Strain in Graphene by Raman Spectroscopy: G Peak Splitting, Gruneisen Parameters, and Sample Orientation. *Phys. Rev. B* **2009**, *79*, 205433.

(20) Huang, M. Y.; Yan, H. G.; Chen, C. Y.; Song, D. H.; Heinz, T. F.; Hone, J. Phonon Softening and Crystallographic Orientation of Strained Graphene Studied by Raman Spectroscopy. *Proc. Natl. Acad. Sci. U. S. A.* **2009**, *106*, 7304−7308.

(21) Huang, M. Y.; Yan, H. G.; Heinz, T. F.; Hone, J. Probing Strain-Induced Electronic Structure Change in Graphene by Raman Spectroscopy. *Nano Lett.* **2010**, *10*, 4074−4079.

(22) Yoon, D.; Son, Y. W.; Cheong, H. Strain-Dependent Splitting of the Double-Resonance Raman Scattering Band in Graphene. *Phys. Rev. Lett.* **2011**, *106*, 155502.

(23) Lee, J. E.; Ahn, G.; Shim, J.; Lee, Y. S.; Ryu, S. Optical Separation of Mechanical Strain from Charge Doping in Graphene. *Nat. Commun.* **2012**, *3*, 1024.

(24) Ferrari, A. C.; Basko, D. M. Raman Spectroscopy as a Versatile Tool for Studying the Properties of Graphene. *Nat. Nanotechnol* **2013**, *8*, 235−246.

(25) Ahn, G.; Kim, H. R.; Ko, T. Y.; Choi, K.; Watanabe, K.; Taniguchi, T.; Hong, B. H.; Ryu, S. Optical Probing of the Electronic Interaction between Graphene and Hexagonal Boron Nitride. *ACS Nano* **2013**, *7*, 1533−1541.

(26) Zhou, Q.; Coh, S.; Cohen, M. L.; Louie, S. G.; Zettl, A. Imprint of Transition Metal D Orbitals on a Graphene Dirac Cone. *Phys. Rev. B* **2013**, *88*, 235431.

(27) Hwang, J.; Hwang, H.; Kim, M. J.; Ryu, H.; Lee, J. E.; Zhou, Q.; Mo, S. K.; Lee, J.; Lanzara, A.; Hwang, C. Hole Doping, Hybridization Gaps, and Electronic Correlation in Graphene on a Platinum Substrate. *Nanoscale* **2017**, *9*, 11498−11503.

(28) Usachov, D. Y.; Davydov, V. Y.; Levitskii, V. S.; Shevelev, V. O.; Marchenko, D.; Senkovskiy, B. V.; Vilkov, O. Y.; Rybkin, A. G.; Yashina, L. V.; Chulkov, E. V.; et al. Raman Spectroscopy of Lattice-Matched Graphene on Strongly Interacting Metal Surfaces. *ACS Nano* **2017**, *11*, 6336−6345.

(29) Fleischmann, M.; Hendra, P. J.; Mcquillan, A. J. Raman-Spectra of Pyridine Adsorbed at a Silver Electrode. *Chem. Phys. Lett.* **1974**, *26*, 163−166.

(30) Moskovits, M. Surface-Enhanced Spectroscopy. *Rev. Mod. Phys.* **1985**, *57*, 783−826.

(31) Kneipp, K.; Wang, Y.; Kneipp, H.; Perelman, L. T.; Itzkan, I.; Dasari, R.; Feld, M. S. Single Molecule Detection Using Surface-Enhanced Raman Scattering (Sers). *Phys. Rev. Lett.* **1997**, *78*, 1667−1670.
(32) Nie, S. M.; Emory, S. R. Probing Single Molecules and Single Nanoparticles by Surface-Enhanced Raman Scattering. *Science* **1997**, *275*, 1102−1106.
(33) Stockle, R. M.; Suh, Y. D.; Deckert, V.; Zenobi, R. Nanoscale Chemical Analysis by Tip-Enhanced Raman Spectroscopy. *Chem. Phys. Lett.* **2000**, *318*, 131−136.
(34) Pettinger, B.; Ren, B.; Picardi, G.; Schuster, R.; Ertl, G. Nanoscale Probing of Adsorbed Species by Tip-Enhanced Raman Spectroscopy. *Phys. Rev. Lett.* **2004**, *92*, 096101.
(35) Wu, D. Y.; Li, J. F.; Ren, B.; Tian, Z. Q. Electrochemical Surface-Enhanced Raman Spectroscopy of Nanostructures. *Chem. Soc. Rev.* **2008**, *37*, 1025−1041.
(36) Stiles, P. L.; Dieringer, J. A.; Shah, N. C.; Van Duyne, R. R. Surface-Enhanced Raman Spectroscopy. *Annu. Rev. Anal Chem.* **2008**, *1*, 601−626.
(37) Ling, X.; Xie, L. M.; Fang, Y.; Xu, H.; Zhang, H. L.; Kong, J.; Dresselhaus, M. S.; Zhang, J.; Liu, Z. F. Can. Graphene Be Used as a Substrate for Raman Enhancement? *Nano Lett.* **2010**, *10*, 553−561.
(38) Ling, X.; Fang, W. J.; Lee, Y. H.; Araujo, P. T.; Zhang, X.; Rodriguez-Nieva, J. F.; Lin, Y. X.; Zhang, J.; Kong, J.; Dresselhaus, M. S. Raman Enhancement Effect on Two-Dimensional Layered Materials: Graphene, H-Bn and Mos2. *Nano Lett.* **2014**, *14*, 3033−3040.
(39) Langer, J.; de Aberasturi, D. J.; Aizpurua, J.; Alvarez-Puebla, R. A.; Auguie, B.; Baumberg, J. J.; Bazan, G. C.; Bell, S. E. J.; Boisen, A.; Brolo, A. G.; et al. Present and Future of Surface-Enhanced Raman Scattering. *ACS Nano* **2020**, *14*, 28−117.
(40) Calizo, I.; Bejenari, I.; Rahman, M.; Liu, G.; Balandin, A. A. Ultraviolet Raman Microscopy of Single and Multilayer Graphene. *J. Appl. Phys.* **2009**, *106*, 043509.
(41) Costa, S. D.; Righi, A.; Fantini, C.; Hao, Y. F.; Magnuson, C.; Colombo, L.; Ruoff, R. S.; Pimenta, M. A. Resonant Raman Spectroscopy of Graphene Grown on Copper Substrates. *Solid State Commun.* **2012**, *152*, 1317−1320.
(42) Liu, H. L.; Siregar, S.; Hasdeo, E. H.; Kumamoto, Y.; Shen, C. C.; Cheng, C. C.; Li, L. J.; Saito, R.; Kawata, S. Deep-Ultraviolet Raman Scattering Studies of Monolayer Graphene Thin Films. *Carbon* **2015**, *81*, 807−813.
(43) Yin, X. L.; Li, Y. L.; Ke, F.; Lin, C. F.; Zhao, H. B.; Gan, L.; Luo, Z. T.; Zhao, R. G.; Heinz, T. F.; Hu, Z. H. Evolution of the Raman Spectrum of Graphene Grown on Copper Upon Oxidation of the Substrate. *Nano Res.* **2014**, *7*, 1613−1622.
(44) Lien, D. H.; Kang, J. S.; Amani, M.; Chen, K.; Tosun, M.; Wang, H. P.; Roy, T.; Eggleston, M. S.; Wu, M. C.; Dubey, M.; et al. Engineering Light Outcoupling in 2d Materials. *Nano Lett.* **2015**, *15*, 1356−1361.
(45) Yoon, D.; Moon, H.; Son, Y. W.; Samsonidze, G.; Park, B. H.; Kim, J. B.; Lee, Y.; Cheong, H. Strong Polarization Dependence of Double-Resonant Raman Intensities in Graphene. *Nano Lett.* **2008**, *8*, 4270−4274.
(46) Heeg, S.; Fernandez-Garcia, R.; Oikonomou, A.; Schedin, F.; Narula, R.; Maier, S. A.; Vijayaraghavan, A.; Reich, S. Polarized Plasmonic Enhancement by Au Nanostructures Probed through Raman Scattering of Suspended Graphene. *Nano Lett.* **2013**, *13*, 301−308.
(47) Yu, V.; Whiteway, E.; Maassen, J.; Hilke, M. Raman Spectroscopy of the Internal Strain of a Graphene Layer Grown on Copper Tuned by Chemical Vapor Deposition. *Phys. Rev. B* **2011**, *84*, 205407.
(48) Kang, J. H.; Moon, J.; Kim, D. J.; Kim, Y.; Jo, I.; Jeon, C.; Lee, J.; Hong, B. H. Strain Relaxation of Graphene Layers by Cu Surface Roughening. *Nano Lett.* **2016**, *16*, 5993−5998.
(49) Deng, B.; Wu, J. X.; Zhang, S. S.; Qi, Y.; Zheng, L. M.; Yang, H.; Tang, J. L.; Tong, L. M.; Zhang, J.; Liu, Z. F.; et al. Anisotropic Strain Relaxation of Graphene by Corrugation on Copper Crystal Surfaces. *Small* **2018**, *14*, 1800725.
(50) Yi, D.; Luo, D.; Wang, Z. J.; Dong, J. C.; Zhang, X.; Willinger, M. G.; Ruoff, R. S.; Ding, F. What Drives Metal-Surface Step Bunching in Graphene Chemical Vapor Deposition? *Phys. Rev. Lett.* **2018**, *120*, 246101.
(51) Matsuda, N.; Yoshii, K.; Ataka, K.; Osawa, M.; Matsue, T.; Uchida, I. Surface-Enhanced Infrared and Raman Studies of Electrochemical Reduction of Self-Assembled Monolayers Formed from Para-Nitrohiophenol at Silver. *Chem. Lett.* **1992**, *21*, 1385−1388.
(52) Huang, Y. F.; Zhang, M.; Zhao, L. B.; Feng, J. M.; Wu, D. Y.; Ren, B.; Tian, Z. Q. Activation of Oxygen on Gold and Silver Nanoparticles Assisted by Surface Plasmon Resonances. *Angew. Chem. Int. Edit* **2014**, *53*, 2353−2357.

Recommended by ACS

Fast Twist Angle Mapping of Bilayer Graphene Using Spectroscopic Ellipsometric Contrast Microscopy

Teja Potočnik, Jack A. Alexander-Webber, *et al.*

JUNE 08, 2023
NANO LETTERS

READ

Observation of Robust and Long-Ranged Superperiodicity of Electronic Density Induced by Intervalley Scattering in Graphene/Transition Metal Dichalcogenide Heterostructures

Mo-Han Zhang, Lin He, *et al.*

APRIL 03, 2023
NANO LETTERS

READ

In Situ Growth Dynamics of Uniform Bilayer Graphene with Different Twisted Angles Following Layer-by-Layer Mode

Wei Wei, Yi Cui, *et al.*

NOVEMBER 29, 2022
THE JOURNAL OF PHYSICAL CHEMISTRY LETTERS

READ

Surface Functionalization of Substrate-Transferred Graphene for Electronic Applications

Jing-jiang Yu, Armen Gulian, *et al.*

MAY 03, 2023
ACS APPLIED NANO MATERIALS

READ

Get More Suggestions >

https://doi.org/10.1021/acs.jpclett.3c01074
J. Phys. Chem. Lett. 2023, 14, 5573−5579